3-D Least Squares Matching for Volumetric Velocimetry Data Processing

Patrick Westfeld[1], Hans-Gerd Maas[1], Oliver Pust[2], Jens Kitzhofer[3], Christoph Brücker[3]

1: Institute of Photogrammetry and Remote Sensing, Technische Universität Dresden, Germany,
{patrick.westfeld,hans-gerd.maas}@tu-dresden.de
2: Dantec Dynamics A/S, Skovlunde, Denmark, oliver.pust@dantecdynamic.com
3: Insitute of Mechanics and Fluid Dynamics, Technische Universität Bergakademie Freiberg, Germany,
{kitzhofer,bruecker}@imfd.tu-freiberg.de

Abstract   The paper presents a three-dimensional least squares matching approach applied to time-resolved volumetric particle image velocimetry data to determine 3-D velocity fields. It will introduce the functional and stochastic model of the tracking algorithm which includes the geometric concept, the parameterization of the transformation, the derivation of information on precision, determinability and reliability of the transformation parameters as well as the integration of additional constraints. The implementation of 3-D least squares matching has been validated with both simulated and real data. The accuracy potential as well as the reliability will be documented comparatively for all data sets. The parameterization for different flows and the percentage of significant parameters in accepted trajectories will be analyzed and a comparison between 3-D cross correlation and 3-D least squares matching is given.

1. Introduction

Photogrammetric 3-D motion analysis is a well-established field of close-range photogrammetry and allows the extraction of geometric information from images with high precision and reliability. In this context, least squares techniques such as least squares matching depict powerful, flexible and widely used tools for the computation of velocity vectors from 2-D or 3-D image sequences.

Volumetric PIV generates a tomographic reconstruction of a particle constellation from a limited number of synchronized camera views by applying a feasible reconstruction algorithm like MART (Herman & Lent, 1976) or MinART (Maas et al., 2009). The advantage of PIV is the insensitivity to high seeding densities. This kind of tomographic reconstruction facilitates the implementation of a volume-based particle tracking technique rather than a discrete PTV (particle tracking velocimetry) approach, which may be prone to ambiguities at high seeding densities (Papantoniou & Dracos, 1989).

Volume-based tracking techniques deliver dense flow velocity field information by dividing time-resolved volumetric velocimetry data into cuboids of a predefined size and tracking these cuboids through the reconstructed sequence of voxel spaces. Herein, 3-D cross correlation (3-D CC, Keane & Adrian, 1992) is a rather straightforward technique to determine 3-D displacement vectors between cuboids of two consecutive epochs with sub-voxel precision by calculating a 3-D cross correlation coefficient field and fitting a Gaussian function into it to obtain sub-voxel accuracy. An implementation of this approach is quite simple but limited to the determination of the shifts in each direction only. Thus, cuboids with significant deformations will not be tracked reliably. Scarano (2002) partially improves this by iterative image deformation methods, but at much larger computational efforts. Here, 3-D least squares matching (3-D LSM) offers the advantage of being

adaptive to cuboid deformation, rotation and shear, which makes it a rather interesting alternative to 3-D CC.

2. Principle

3-D least squares matching (3-D LSM) is a volumetric matching technique (Maas et al., 1994). In analogy to 2-D least squares matching (Ackermann, 1984; Förstner, 1984; Grün, 1985), 3-D LSM utilizes an iterative geometric and radiometric transformation between two (or more) consecutive cuboids in a way that the sum of the squares of the gray value differences between the voxels of the cuboids reaches a minimum. The geometric transformation is a 3-D affine transformation with 12 parameters, the optional radiometric adjustment may use a 2-parameters linear correction term (Fig. 1).
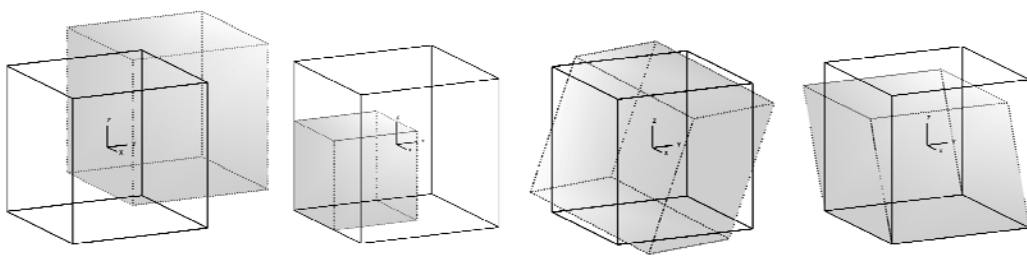

Fig 1.   3-D affine transformation of a cuboid. From left to right: translation, scale, rotation, shear.

The essential advantage of these additional non-translational cuboid transformation parameters is the adaptivity to changes in scale, rotation or shear. If not considered, they may hamper the determination of velocity vectors or systematically deteriorate the quality or results.

Compared to the 3-D cross correlation (3-D CC) method, cuboid tracking formulated as a least squares problem has the following implications:

- The geometric transformation includes additional scale, shear and rotation parameters. These parameters allow adapting to linear deformations of cuboids.

- The mathematical model can be extended by additional information or constraints. When applied to liquid flow data, an incompressibility constraint has to be introduced to force the volume of a cuboid to remain constant during the iterative transformation.

- Assuming a correct mathematical model and sufficient contrast within the cuboids, 3-D LSM can achieve very high sub-voxel precision down to $^{1}/_{100}$ of a voxel.

- 3-D LSM converges in a few iterations and may reduce the computational effort.

- The observation equations are non-linear. The linearized equations requires initial values, usually obtained by pre-knowledge or by hierarchically applying the technique on a resolution pyramid.

- The adjustment has a high redundancy, allowing for general acceptance decisions and the detection and elimination of outliers.

- Accuracy estimates of the unknown parameters can be delivered.

3. Mathematical Model

3.1 Functional Model

Template cuboid $\mathbf{g_1}$ and search cuboid $\mathbf{g_2}$, taken from consecutive volume data sets Υ_1 and Υ_2, provide gray value observations for the adjustment at each position $(x,y,z)_1$ resp. $(x,y,z)_2$. The geometric and radiometric relations between those cuboids can be formulated as

$$g_1(x,y,z) - e(x,y,z) = r_0 + r_1 \cdot g_2(x,y,z) \tag{1}$$

whereas r_0 and r_1 model changes in brightness and contrast, and $\mathbf{e}$ considers a small noise fraction. The geometric 3-D affine transformation model is given by

$$
\begin{aligned}
x_2 &= a_0 + a_1 x_1 + a_2 y_1 + a_3 z_1 \\
y_2 &= b_0 + b_1 x_1 + b_2 y_1 + b_3 z_1 \\
z_2 &= c_0 + c_1 x_1 + c_2 y_1 + c_3 z_1
\end{aligned}
\tag{2}
$$

with (a_0,b_0,c_0) being shifts, (a_1,b_2,c_3) scales, and $(a_2,a_3,b_1,b_3,c_1,c_2)$ rotations and shears. Within a Gauss-Markov Model (GMM), the parameters can be estimated by minimizing the sum of the squares of the gray value differences between $\mathbf{g_1}$ and $\mathbf{g_2}$.

Suppose approximate values are available for all introduced parameters of the cuboid $\mathbf{g_2}$ at its initial position $\mathbf{g_2}^0$, Eq. 1 can be linearized as

$$g_1(x,y,z) - e(x,y,z) = g_2^0(x,y,z) + \frac{\partial g_2^0(x,y,z)}{\partial x} dx + \frac{\partial g_2^0(x,y,z)}{\partial y} dy + \frac{\partial g_2^0(x,y,z)}{\partial z} dz \tag{3}$$

with

$$dx = (\partial x / \partial p_i) \cdot dp_i, \; dy = (\partial y / \partial p_i) \cdot dp_i, \; dz = (\partial z / \partial p_i) \cdot dp_i, \quad p_i \in (a_j, b_j, c_j r_0, r_1), \; j = \{0,1,2,3\} \tag{4}$$

With the gray value gradients in three coordinate directions

$$g_x = \frac{\partial g_2^0(x,y,z)}{\partial x}, \; g_y = \frac{\partial g_2^0(x,y,z)}{\partial y}, \; g_z = \frac{\partial g_2^0(x,y,z)}{\partial z} \tag{5}$$

this leads to a linearized observation equation

$$
\begin{aligned}
\Phi(p_i) = g_1(x,y,z) - e(x,y,z) = g_2^0(x,y,z) &+ g_x da_0 + g_x x_2^0 da_1 + g_x y_2^0 da_2 + g_x z_2^0 da_3 \\
&+ g_y db_0 + g_y x_2^0 db_1 + g_y y_2^0 db_2 + g_y z_2^0 db_3 \\
&+ g_z dc_0 + g_z x_2^0 dc_1 + g_z y_2^0 dc_2 + g_z z_2^0 dc_3 \\
&+ r_0 + r_1 g_2^0(x,y,z)
\end{aligned}
\tag{6}
$$

Like all non-linear least squares approaches, the estimation of the unknowns takes place in an iterative way. They are updated after each iteration until a preset iteration criteria has been reached.

In general, the residual amounts are non-integer values and the gray values in the search cuboid will need to be determined by interpolation.

For the special case of tracking particles in liquids, a cuboid, while changing its shape due to deformations, will have a constant volume. Consequentially, a volume constraint was implemented to consider the incompressibility of the liquid. The incompressibility constraint is formulated as

$$a_1 \cdot b_2 \cdot c_3 = 1 \tag{7}$$

and results in one additional linearized equation for the GMM:

$$\Psi(p_i) = \frac{\partial \Psi(p_i^0)}{\partial a_1} da_1 + \frac{\partial \Psi(p_i^0)}{\partial b_2} db_2 + \frac{\partial \Psi(p_i^0)}{\partial c_3} dc_3 = 0 \tag{8}$$

3.2 Stochastic Model

The stochastic model describes the variances and co-variances of the observations. In the present case, homogeneous data are available and all gray value observations are introduced with same a-priori accuracy specifications in terms of equal variances resp. equal stochastic weights.

$$\mathop{\mathbf{P}}_{n,n} = \begin{bmatrix} s_0^2/s_1^2 & & & \\ & s_0^2/s_2^2 & & \\ & & \ddots & \\ & & & s_0^2/s_n^2 \end{bmatrix} = \mathop{\mathbf{I}}_{n,n} \tag{9}$$

where s_0 is the a-priori standard deviation of unit weight and s_i is the a-priori standard deviation of the observation k, $k=\{1,2,...,n\}$. Due to independent and homogeneous observations, the weight matrix of the observations $\mathbf{P}$ will often be an identity matrix $\mathbf{I}$ ($s_0 = s_i \equiv 1$).

The incompressibility constraint (Eq. 7) is introduced with highest priority by setting its a-priori standard deviation to 'zero' ($s_\Psi \equiv 0$, $\mathbf{P}_\Psi \equiv 0$).

3.3 Gauss-Markov Model

Each voxel i in a cuboid produces one observation equation Φ_i. For each consecutive pair of cuboids, $c = 1$ additional equation has to be set up, which considers the incompressibility constraint Ψ. The complete equation system is solved in an extended Gauss-Markov Model (conditional least squares adjustment) to estimate u unknown transformation parameters by n gray value observations per cuboid:

$$\mathop{\mathbf{v}}_{n,1} = \mathop{\mathbf{A}}_{n,u} \mathop{\hat{\mathbf{x}}}_{u,1} - \mathop{\mathbf{l}}_{n,1}$$
$$\mathop{\mathbf{w}}_{c,1} = \mathop{\mathbf{B}}_{c,u} \mathop{\hat{\mathbf{x}}}_{u,1} \tag{10}$$

Assuming normal distributed errors, the following conditions for the residuals $\mathbf{v}$ resp. the inconsistencies $\mathbf{w}$ results

$$\mathbf{v}^T \mathbf{P} \mathbf{v} + 2\mathbf{k}\left(\mathbf{B}\hat{\mathbf{x}} + \mathbf{w}\right) \mapsto \min,$$

which leads to the extended normal system of equations solved for the vector of unknowns:

$$\begin{bmatrix} \hat{\mathbf{x}} \\ \mathbf{k} \end{bmatrix} = \begin{bmatrix} \mathbf{A}^T\mathbf{P}\mathbf{A} & \mathbf{B}^T \\ \mathbf{B} & -\mathbf{P}_\Psi^{-1} \end{bmatrix} \begin{bmatrix} \mathbf{A}^T\mathbf{P}\mathbf{l} \\ \mathbf{w} \end{bmatrix} \tag{11}$$

Herein, the Jacobian matrix **A** consists of the derivatives of $\Phi(p_i)$ (Eq. 6) with respect to the unknowns and describes the functional relation between the parameters. In analogous way to the observation equations, **B** consists of the derivatives of $\Psi(p_i)$ (Eq. 8).

$$\mathbf{A}_{n,u} = \begin{bmatrix} \frac{\partial\Phi_1}{\partial a_0} & \frac{\partial\Phi_1}{\partial a_1} & \frac{\partial\Phi_1}{\partial a_2} & \frac{\partial\Phi_1}{\partial a_3} & \frac{\partial\Phi_1}{\partial b_0} & \frac{\partial\Phi_1}{\partial b_1} & \frac{\partial\Phi_1}{\partial b_2} & \frac{\partial\Phi_1}{\partial b_3} & \frac{\partial\Phi_1}{\partial c_0} & \frac{\partial\Phi_1}{\partial c_1} & \frac{\partial\Phi_1}{\partial c_2} & \frac{\partial\Phi_1}{\partial c_3} & \frac{\partial\Phi_1}{\partial r_0} & \frac{\partial\Phi_1}{\partial r_1} \\ \frac{\partial\Phi_2}{\partial a_0} & \frac{\partial\Phi_2}{\partial a_1} & \frac{\partial\Phi_2}{\partial a_2} & \frac{\partial\Phi_2}{\partial a_3} & \frac{\partial\Phi_2}{\partial b_0} & \frac{\partial\Phi_2}{\partial b_1} & \frac{\partial\Phi_2}{\partial b_2} & \frac{\partial\Phi_2}{\partial b_3} & \frac{\partial\Phi_2}{\partial c_0} & \frac{\partial\Phi_2}{\partial c_1} & \frac{\partial\Phi_2}{\partial c_2} & \frac{\partial\Phi_2}{\partial c_3} & \frac{\partial\Phi_2}{\partial r_0} & \frac{\partial\Phi_2}{\partial r_1} \\ \vdots & \vdots & \vdots & \vdots & \vdots & \vdots & \vdots & \vdots & \vdots & \vdots & \vdots & \vdots & \vdots & \vdots \\ \frac{\partial\Phi_n}{\partial a_0} & \frac{\partial\Phi_1}{\partial a_1} & \frac{\partial\Phi_n}{\partial a_2} & \frac{\partial\Phi_n}{\partial a_3} & \frac{\partial\Phi_n}{\partial b_0} & \frac{\partial\Phi_n}{\partial b_1} & \frac{\partial\Phi_n}{\partial b_2} & \frac{\partial\Phi_n}{\partial b_3} & \frac{\partial\Phi_n}{\partial c_0} & \frac{\partial\Phi_n}{\partial c_1} & \frac{\partial\Phi_n}{\partial c_2} & \frac{\partial\Phi_n}{\partial c_3} & \frac{\partial\Phi_n}{\partial r_0} & \frac{\partial\Phi_n}{\partial r_1} \end{bmatrix} \tag{12}$$

$$\mathbf{B}_{c,u} = \begin{bmatrix} 0 & \frac{\partial\Psi_1}{\partial a_1} & 0 & 0 & 0 & 0 & \frac{\partial\Psi_1}{\partial b_2} & 0 & 0 & 0 & 0 & \frac{\partial\Psi_1}{\partial c_3} & 0 & 0 \end{bmatrix}$$

The vector **l** is denoted as the vector of the reduced observations:

$$l_n = \begin{bmatrix} g_{1,1} - g_{2,1} \\ g_{1,2} - g_{2,2} \\ \vdots \\ g_{1,n} - g_{2,n} \end{bmatrix} \tag{13}$$

The vector of Lagrangian multipliers **k** are not normally of interest. The vector of the unknowns contains the estimated parameters:

$$\hat{\mathbf{x}}_u = \begin{bmatrix} a_0 & a_1 & a_2 & a_3 & b_0 & b_1 & b_2 & b_3 & c_0 & c_1 & c_2 & c_3 & r_0 & r_1 \end{bmatrix}^T \tag{14}$$

4. Internal Quality Measures

As a least squares adjustment method, 3-D least squares matching (3-D LSM) delivers information on the precision, determinability and reliability of the 12 affine transformation parameters. This includes the standard deviation of each of the parameters as well as the correlation between parameters.

The a-posteriori standard deviation of unit weight is given by

$$\hat{s}_0 = \sqrt{\frac{\mathbf{v}^T\mathbf{P}_{valid}\mathbf{v}}{r}} \tag{15}$$

with an redundancy $r = n - u + c$.

The a-posteriori standard deviation of an estimated parameter i is given by

$$\hat{s}_i = \hat{s}_0 \sqrt{q_{ii}} \qquad (16)$$

where q_{ii} is the ith diagonal element of the cofactor matrix $\mathbf{Q} = \left(\mathbf{A}^T \mathbf{P} \mathbf{A}\right)^{-1}$.

Furthermore, the level of significance can be calculated for each parameter in each cuboid. To decide whether a transformation parameter is significant or not, the one-dimensional Student test function can be calculated for each introduced parameter p_i. The parameters are significant, if

$$t_i = \frac{p_i}{\hat{s}_i} > q \qquad (17)$$

is fulfilled. The quantile q can be obtained by the inverse of the Student's t inverse cumulative distribution function using the degrees of freedom r and a given probability P that the parameters are significant. Non-significant parameters may be excluded from the estimation process (and set to zero) in order to improve the strength of the solution. Assuming at least one non-significant parameter in the introduced set of parameters p_i, the least squares adjustment is repeated until all used parameters are significant.

5. Some Results

5.1 Simulated Data Set

A simulated data set was generated by composing two consecutive voxel spaces Υ_1 resp. Υ_2 with a volume of $(101 \text{ voxel})^3$. These volumetric reconstructions contain the flow of a vortex ring. The second state of the vortex was achieved by a defined translation and rotation of the first one. Further, some random noise was added to the gray values of both voxel spaces.

The velocity field information were determined comparatively by 3-D cross correlation (3-D CC) and 3-D least squares matching (3-D LSM). A regular grid of 17^3 voxel cuboids was defined into Υ_1. For each grid position, the corresponding cuboids were determined either by calculation the 3-D cross correlation coefficients or by calculating the 3-D LSM affine transformation parameters. All tracking results were accepted. Neither a threshold for the cross correlation coefficient nor 3-D LSM outlier criteria were applied.

For 3-D CC, the template cuboid $\mathbf{g}_1$ was shifted through the search volume Υ_2. At each position the normalized cross correlation coefficients between the gray values of the template $\mathbf{g}_1$ and the corresponding search cuboid $\mathbf{g}_2$ were calculated. A Gaussian function was fitted into the computed 3-D cross correlation coefficient field to obtain sub-voxel accuracy. The position with the highest coefficient represents the location of $\mathbf{g}_1$ in Υ_2. For 3-D LSM, the 12 parameters of the 3-D affine transformation were computed as described in Sec. 3. Parameters were excluded from the transformation if they turned out insignificant in the significance test (Sec. 4).
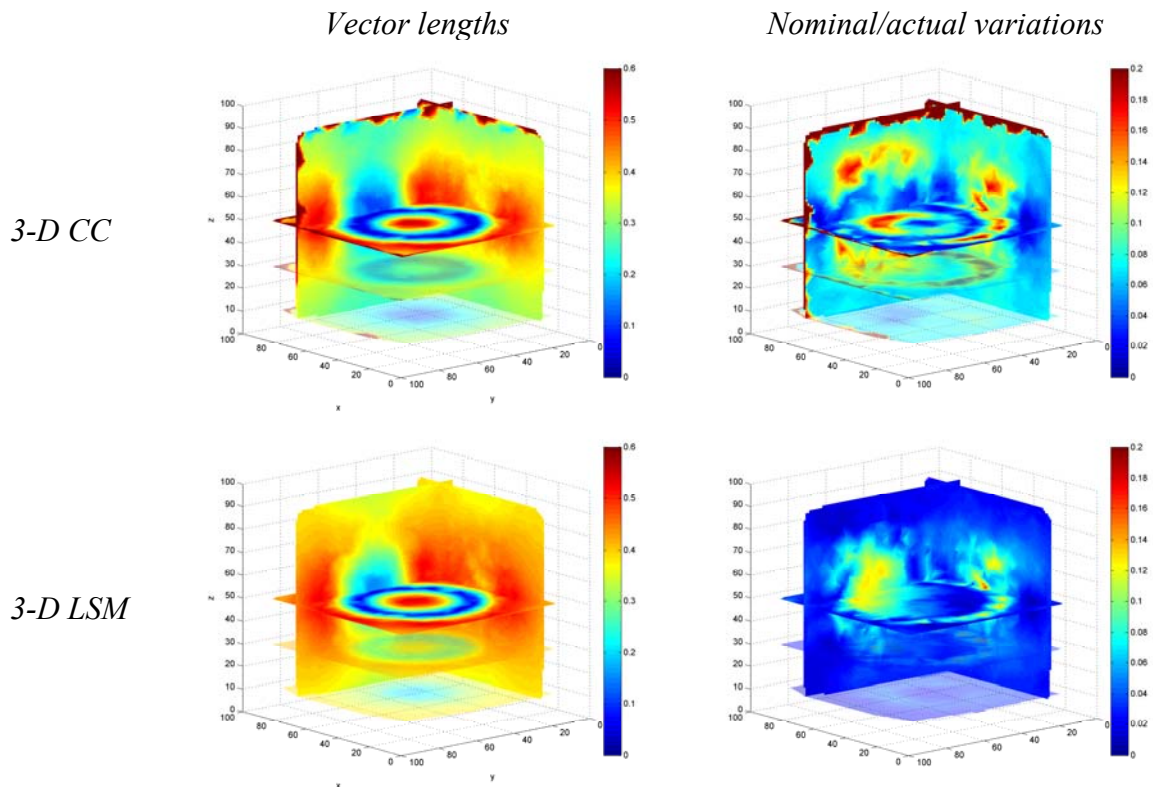
Vector lengths   *Nominal/actual variations*

3-D CC

3-D LSM

Fig 2.   Cross sections of color-coded vector lengths (left) and nominal/actual variations (right) of a simulated vortex ring achieved by 3-D CC (top) and 3-D LSM (bottom).

The results can be seen in Fig. 2 and Tab. 1. At first the cross sections of the resulting velocity vector fields looks similar for 3-D CC and 3-D LSM. Analyzing the variations between the nominal and actual particle positions show the great advantage of 3-D LSM. In contrast to 3-D CC, the trajectories were determined more precisely and reliability. Mainly in the center of the vortex, an improved precision by factor 2-6 can be achieved, which proves the relevance of determining not only translation parameters in cuboid tracking.

	$\sigma_{\Delta x}$	$\sigma_{\Delta y}$	$\sigma_{\Delta z}$
3-D CC	1.1182e-001	1.1566e-001	1.6526e-001
3-D LSM	1.7027e-002	1.6948e-002	4.3520e-002

Tab. 1   Standard deviations of actual/nominal variations in *x*, *y* and *z* (in voxel).

5.2 Real Data Set

The real data set originates from the following experimental setup: A vortex ring in a water tank is illuminated by a 3-D laser beam device. A rotating mirror generates parallel light sheet planes with a thickness of 10 mm. This volume of about $(10 \times 10 \times 1)$ cm^3 is recorded by a system of four synchronized high speed cameras (1024×1024 pixel, 1000 fps) equipped with telecentric lenses (Fig. 3 and 5). Neutrally buoyant seeding particles are injected into the center of a vortex generator. See (Kitzhofer et al., 2009) for detailed specifications of this experimental setup.
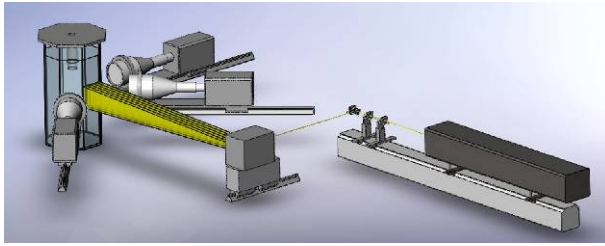
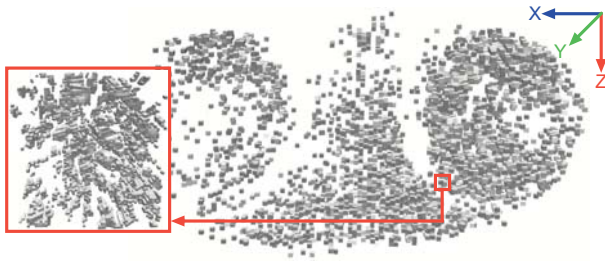**Fig. 3.** Experimental setup with telecentric lenses (Kitzhofer et al., 2009).

Fig. 4. Voxel space of the volumetric reconstruction at one epoch (Westfeld & Maas, 2010).
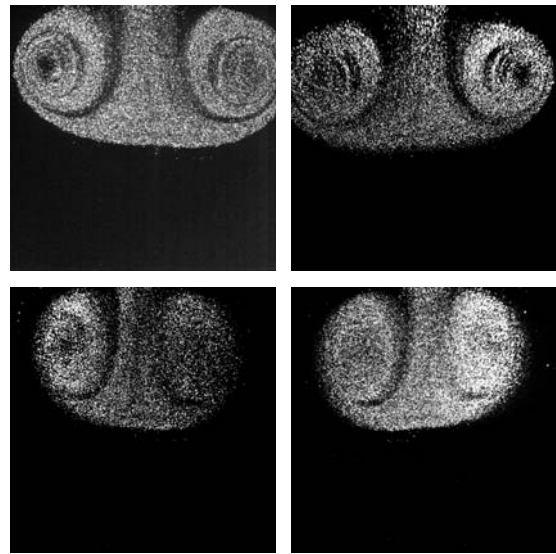
Fig. 5. Vortex ring imaged with four cameras at one epoch (Maas et al., 2009).

The volumetric reconstruction (Fig. 4) results from improved reconstruction techniques presented in (Maas et al., 2009) and (Westfeld & Maas, 2010). The process bases on a multiple projective transformation of each camera view into each depth layer of a the voxel representation of the object space and a MinART (minstore algebraic reconstruction technique) to fill-up the voxel space with gray value information.

The velocity field information can then be obtained by applying the presented 3-D LSM to the time-resolved voxel space representation. Again, a regular grid of 25^3 cuboids was defined into the volumetric reconstruction of $(278 \times 1112 \times 944)$ voxel^3 and the 12 affine parameter were determined. The initial values for all parameters were computed automatically by applying 3-D LSM successively on a 2-level pyramid of the object space. If adequate initial values are available, 3-D LSM converges in a few iterations (Fig. 6 and 7). Non-significant parameters were excluded. Trajectories which do not fulfill the criteria of an outlier detection scheme were removed:

- Affine transformation parameter standard deviation: The results of cuboids with standard deviations exceeding a preset threshold were deleted.

- Convergence behavior: Cuboids with a diverging or oscillating solution were rejected.

- Vector length: Translation vectors exceeding a preset threshold were eliminated.

- Neighborhood correlation: The differences of the translation vector components between neighboring cuboids were analyzed. Vectors with deviations from their neighborhood exceeding a preset limit were eliminated.
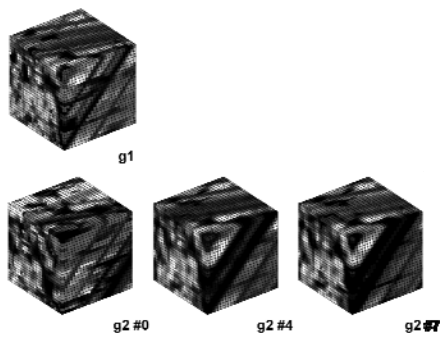
Fig. 6. Template cuboid g_1 and search cuboids g_2 through seven iterations.
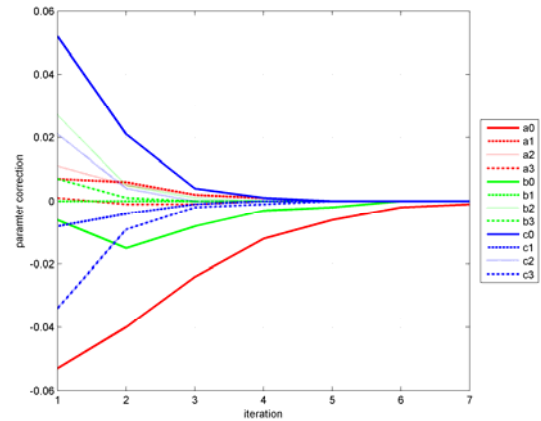
Fig. 7. Convergence behavior of all 12 affine transformation parameters.

The following figures visualize the 3-D LSM results. Fig. 8 shows the cross sections of color-coded velocity in voxel space. Fig. 9 shows the direction of the velocity vectors for one half of the vortex ring in frontal view.
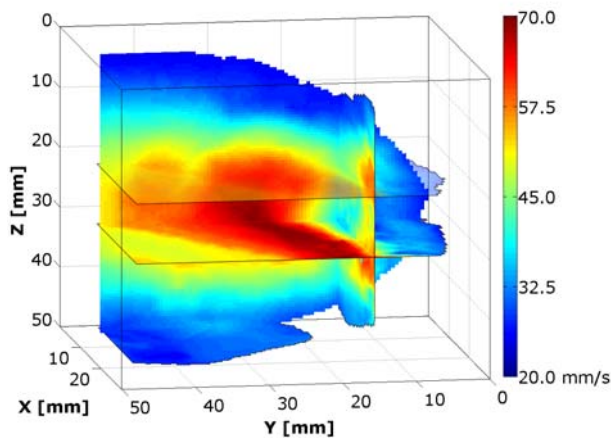

Fig. 8. Cross sections of color-coded velocity in voxel space (Maas et al., 2009).
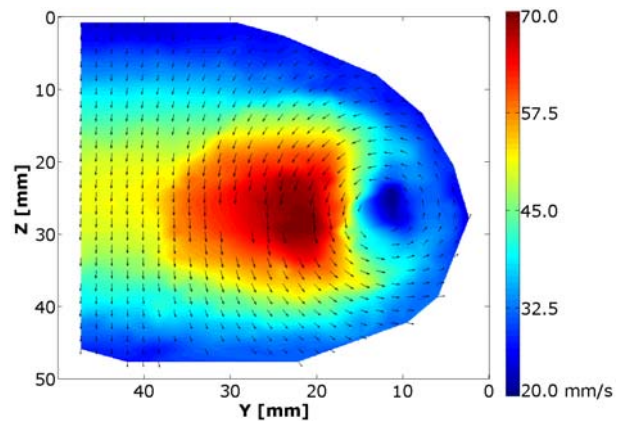
Fig. 9. Cross sections of color-coded velocity in voxel space (Maas et al., 2009).

The standard deviation of unit weight was 2.5 gray values, avaraged over all accepted cuboids. Tab. 2 shows the average standard deviations of the 12 affine transformation parameters. As one can see, the internal precision of the cuboid translation parameters is in the order of $1/100$ of a voxel. However, one has to consider that these internal precision figures are only realistic if the assumed functional and stochastic model is correct (3-D affine transformation and least squares adjustment assuming Gaussian error distribution). Furthermore, Tab. 2 gives an overview on the percentage of significant 3-D affine transformation parameters over all accepted cuboids. As the cuboid translation parameters (a_0,b_0,c_0) were not excluded as a rule in the significance tests, they all have 100% here. The scale parameters (a_1,b_2,c_3), constrained by the incompressibility condition, were only significant in relatively few cuboids, while the rotation and shear parameters (a_2,a_3,b_1,b_3,c_1,c_2) were significant especially in the center of the vortex (Fig. 10). In total, about 20% of the cuboids showed at least one significant non-translation parameter, proving the adequateness of the 3-D LSM approach. Further, the gained 3-D LSM non-translation parameters can be used to estimate the 3-D deformation tensor as well as the 3-D rotational tensor directly (Kitzhofer et al., 2010).

	a_0	b_0	c_0		
$\sigma_i = [vx]$	0.0132	0.0105	0.009		
Sig = [%]	100	100	100		

	a_1	b_2	c_3		
$\sigma_i = [vx]$	2.4e-3	1.8e-3	1.6e-3		
Sig = [%]	1.95	2.68	3.75		

	a_2	a_3	b_1	b_3	c_1	c_2
$\sigma_i = [vx]$	2.4e-3	2.3e-3	1.7e-3	1.8e-3	1.6e-3	1.6e-3
Sig. = [%]	4.42	10.47	6.40	10.77	6.07	12.61

Tab. 2 Average standard deviations of transformation parameters and percentage of significant parameters in accepted trajectories.
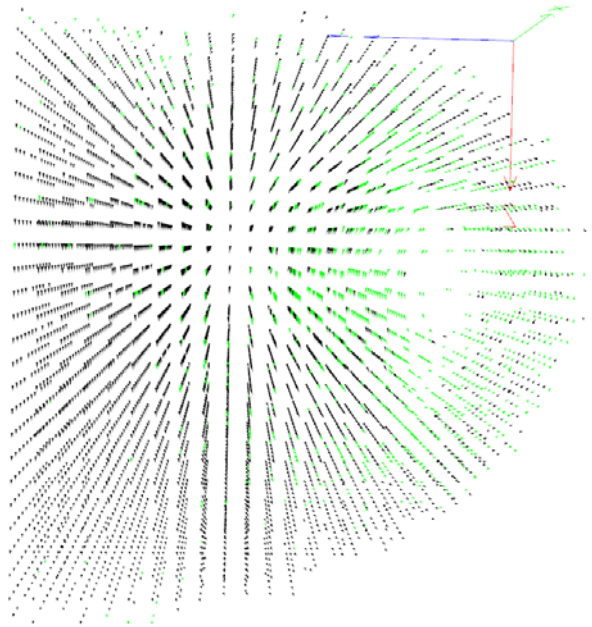

Fig.10. Velocity vector display with vectors belonging to cuboids with at least one significant non-translation 3-D affine transformation parameter coded in green (Maas et al., 2009).

6. Outlook

The paper presented a volume based tracking technique to compute Eulerian 3-D velocity field information from time-resolved voxel space representations. Mainly due to its adaptivity to cuboid deformation and rotation, 3-D least squares matching (3-D LSM) forms a rather interesting alternative to conventional 3-D cross correlation. It was shown that an increase in precision and reliability can be achieved, if scale, rotation and shear information were considered in the tracking process. Moreover, these parameters enable the determination of a shear tensor for each interrogation cube.

Future work will concentrate on extension of the linear transformation model in 3-D LSM by

introducing higher order polynomials. The resolution of the velocity field may also be improved by identifying individual particles in voxel space and tracking those particles, using the results of the volume-based tracking as good approximation.

References

Ackermann, F., 1984. High precision digital image correlation. In: Proceedings of the 39th Photogrammetric Week, Schriftenreihe der Universität Stuttgart, Vol. 9, pp. 231-243.

Förstner, W., 1984. Quality assessment of object location and point transfer using digital image correlation techniques. In: International Archives of Photogrammetry, Vol. 25-III, A3, pp. 197-217.

Grün, A., 1985. Adaptive least squares correlation - a powerful image matching technique. In: South African Journal of Photogrammetry, Remote Sensing and Cartography, Vol. 14, pp. 175-187.

Herman, G. T. & Lent, A., 1976. Iterative reconstruction algorithms. Computers in Biology and Medicine, 6:273-294.

Keane, R. D. & Adrian, R. J., 1992. Theory of cross-correlation analysis of piv images. Applied Scientific Research 49(3), pp. 191-215.

Kitzhofer J., Brücker Ch. & Pust O., 2009. Tomo PTV using 3D Scanning Illumination and Telecentric Imaging. Proceedings of the 8th International Symposium on Particle Image Velocimetry, 25-28 August, Melbourne, Victoria, Australia.

Kitzhofer, J., Westfeld, P., Pust, O., Maas, H.-G. & Brücker, Ch., 2010. Direct Estimation of 3D Deformation and Rotation Rate Tensor from Gray Value Weighted Voxel Space via Least Squares Matching. Accepted for publication in the Proceedings of the 15th International Symposium on Applications of Laser Techniques to Fluid Mechanics, 5 – 8 July 2010, Lisbon.

Maas, H.-G., Stefanidis, A. & Grün, A., 1994. From pixels to voxels - tracking volume elements in sequences of 3-d digital images. In International Archives of Photogrammetry and Remote Sensing, Volume 30, 3/2.

Maas, H.-G., Westfeld, P., Putze, T., Bøtkjær, N., Kitzhofer, J., Brücker, C., 2009. Photogrammetric techniques in multi-camera tomographic PIV. In: Soria, J., Atkinson, C. (eds.), Proceedings of the 8th International Symposium on Particle Image Velocimetry, 25-28 August, Melbourne, Victoria, Australia, pp. 599-602.

Papantoniou, D. & Dracos, T., 1989. Analyzing 3-d turbulent motions in open channel flow by use of stereoscopy and particle tracking. In: H.-H. Hernholz and H. E. Fiedler (eds), Advances in Turbulence, Vol. 2, Springer Heidelberg.

Scarano, F., 2002. Iterative image deformation methods in PIV. Measurement Science and Technology 13:R1-R19, IOP Publishing Ltd.

Westfeld, P. & Maas, H.-G., 2010. 3-D Least Squares Tracking in Time-resolved Tomographic Reconstruction of Dense Flow Marker Fields. Accepted for publication in the Proceedings of the Commission V, WG V/1 Symposium 2010, 21 – 24 June 2010, Newcastle.